To IMAGE or to IMAGINE: visualization of parasite migration as a means to support (malaria) parasite vaccine development

Korne, C.M. de


3

Clustering and erratic movement patterns of syringe-injected versus mosquito-inoculated malaria sporozoites underlie decreased infectivity

Clarize M. de Korne, Béatrice M.F. Winkel, Matthias N. van Oosterom, Severine C. Chevalley-Maurel, Krijn M. Houwing, Jeroen C. Sijtsma, Samaneh Azargoshasb, Els Baalbergen, Blandine M.D. Franke-Fayard, Fijs W.B. van Leeuwen, Meta Roestenberg

mSphere 2021. DOI: 10.1128/mSphere.00218-21

ABSTRACT

Malaria vaccine candidates based on live attenuated sporozoites have led to high levels of protection. However, their efficacy critically depends on the sporozoites' capability to reach and infect the host liver. Administration via mosquito inoculation is by far the most potent method for inducing immunity, but highly impractical. Here, we observed that intradermal syringe-injected *Plasmodium berghei* sporozoites (^{syr}SPZ) were three-fold less efficient in migrating to and infecting mouse liver compared to mosquito-inoculated sporozoites (^{msq}SPZ). This was related to a clustered dermal distribution (2-fold decreased median distance between ^{syr}SPZ vs ^{msq}SPZ) and, more importantly, a significantly 1.4-fold slower and more erratic movement pattern. These erratic movement patterns were likely caused by alteration of dermal tissue morphology (>15 µm intercellular gaps) due to injection of fluid and may critically decrease sporozoite infectivity. These results suggest that novel microvolume-based administration technologies hold promise for replicating the success of mosquito-inoculated live attenuated sporozoite vaccines.

INTRODUCTION

Since 2014, the number of cases of malaria worldwide has remained at 200 million annually leading to more than 400 thousand deaths every year, with children in sub-Saharan Africa bearing the greatest burden[1]. This high morbidity and mortality underline the pressing need for an effective vaccine to support control programs. Live attenuated *Plasmodium falciparum (Pf)* sporozoite (SPZ) based vaccine strategies currently are in clinical development (PfSPZ Vaccine, PfSPZ CVac, PfSPZ-GA1[2]) and have the potential of inducing up to 100% sterile immunity[3, 4].

In order to make live attenuated SPZ amenable for large scale immunization, the US-based biotech Sanaria has developed tools to isolate, purify and cryopreserve SPZ for injection. Unfortunately, the dermal or subcutaneous injection of SPZ provided suboptimal protective efficacy[5]. Although much better efficacy was obtained when injecting high numbers of SPZ intravenously[6], the intradermal, intramuscular or subcutaneous administration routes of low numbers of SPZ are preferred to facilitate global administration to infants in endemic countries at a low cost-of-goods. Better understanding of the differences between the potent mosquito-inoculated SPZ and the unsuccessful syringe-injected SPZ is needed to boost the development of practical and efficacious attenuated SPZ vaccines.

The potency of attenuated SPZ vaccines critically depends on the ability of the SPZ to migrate to and infect the host liver. Transgenic luciferase-expressing SPZ and bioluminescence-based visualization of parasites in mice provide a macroscopic imaging platform to study the liver stage parasite burden after different routes of administration[7]. These studies indicated that mosquito-inoculated SPZ migrate to the liver much more efficiently than intradermally injected SPZ[8-11]. The subsequent development of fluorophore-expressing SPZ and a SPZ fluorescent labelling approach has allowed for more detailed microscopic studies on the motility of individual SPZ, both *in vitro* and in skin[12-14]. Moreover, automated analysis of SPZ motility now provides a platform to quantitatively study SPZ motility under different conditions[15-18].

We aimed to unravel the factors underlying the difference in potency and infectivity between mosquito-inoculated and intradermal syringe-injected SPZ (Scheme 1). For this we microscopically examined the dermal site, quantitatively assessed the distribution of SPZ and their motility patterns after inoculation by mosquito bite (^{msq}SPZ) and injection by needle and syringe (^{syr}SPZ) through automated image analysis. We assessed liver stage parasite burden through bioluminescence assays.

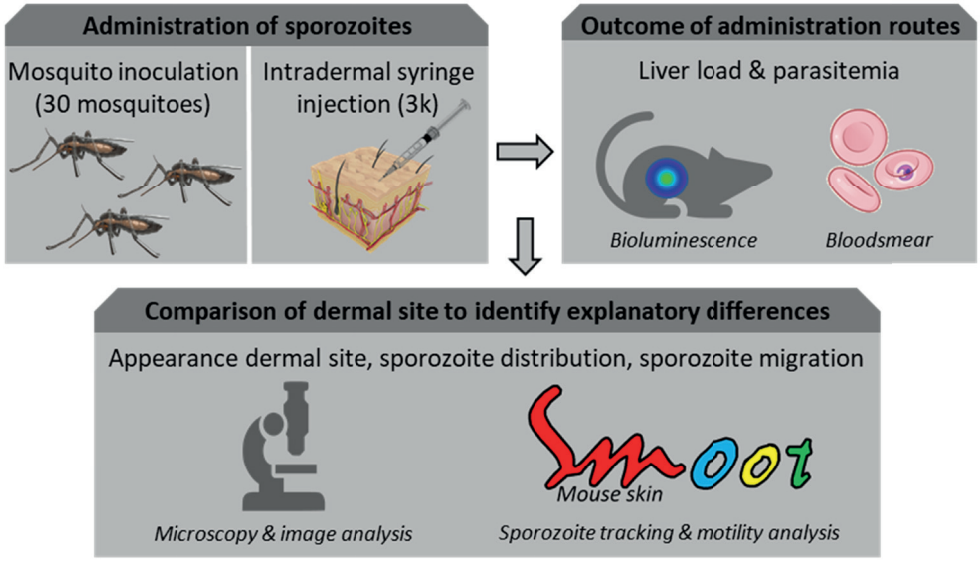

Scheme 1 Study design. SPZ were administered via mosquito inoculation or intradermal syringe injection. Liver load was subsequently assessed by bioluminescence and blood smear patency. Detailed analysis of 1) the appearance of the dermal site, 2) the SPZ distribution and 3) SPZ migration behavior was performed to reveal underlying mechanisms of decreased infectivity.

METHODS

Rodent experiments

Mouse experiments were performed with Female Swiss OF1 mice (6-7 weeks old; Charles River). All animal experiments were granted a license by the Competent Authority after advice on the ethical evaluation by the Animal Experiments Committee Leiden (AVD1160020173304). All experiments were performed in accordance with the Experiments on Animals Act (Wod, 2014), the applicable legislation in the Netherlands and in accordance with the European guidelines (EU directive no. 2010/63/EU) regarding the protection of animals used for scientific purposes. All experiments were performed in a licensed establishment for the use of experimental animals (LUMC). Mice were housed in individually ventilated cages furnished with autoclaved aspen woodchips, fun tunnel, wood chew block and nestlets at 21 ± 2°C under a 12:12 hr light-dark cycle at a relative humidity of 55 ± 10%.

Sporozoite production

Naive mice were infected with the rodent malaria species *P. berghei* as described previously[8]. The transgenic line 1868cl1 expressing mCherry and luciferase under the constitutive HSP70 and eef1a promotors respectively (*Pb*ANKA-mCherry$_{hsp70}$+Luc$_{eef1\alpha}$; line RMgm-1320, www.pberghei.eu) was used. The infected mice were anesthetized and *Anopheles stephensi* female mosquitoes were infected by feeding on the gametocytemic

mice as described previously[19]. The mosquitoes were kept at a temperature of 21 °C and 80% humidity until use.

Sporozoite administration

After anesthetizing mice, *P. berghei* 1868cl1 SPZ were administered using two different methods:

1. ^{msq}SPZ were delivered by shaving the abdomen of the mice and 1 cm^2 skin was exposed for 15 minutes to around 30 infected mosquitoes (exact numbers are specified per experiment). Blood-fed mosquitoes were counted and the presence of SPZ in their salivary glands was confirmed using the quantitative analysis of the luciferase activity after putting the mosquitoes in a 20 µl drop D-luciferin (8 mg/ml in phosphate-buffered saline (PBS)).
2. ^{syr}SPZ were obtained by manual dissection of the salivary glands of infected female *Anopheles stephensi* mosquitoes 20-24 days post infection. The salivary glands were collected and homogenized to release SPZ in Roswell Park Memorial Institute medium (RPMI; Thermo Fisher Scientific) enriched with 10% fetal bovine serum (Life Technologies Inc.). The free SPZ were counted in a Bürker counting chamber using phase-contrast microscopy to prepare the injection samples. Directly after counting (within 45 minutes after crushing), 10 µl sample containing 3000 SPZ was administered by injection into the abdominal skin (within the same region as defined for exposure to mosquitoes) using an insulin syringe (Becton Dickinson, Micro-Fine+, 0.5 ml; 0.30 x 8.0 mm, 30G). The number of SPZ delivered by exposure to 30 infected mosquitoes was considered consistent with intradermal delivery of 3000 SPZ via syringe injection based on available literature (mean number of SPZ inoculated per mosquito: 116 ± 28[20]).

Quantification of parasite liver load and prepatent period

The liver stage of the *P. berghei* infection in 11 mice (6 mice challenged by 33 (IQR: 30-33) mosquito bites of which 25 (IQR: 22-28) contained blood and 5 mice challenged by syringe injection of SPZ) was visualized and quantified by measuring the luciferase activity in the liver at 44 hr after the challenge with SPZ using the IVIS Lumina II Imaging System (Perkin Elmer Life Sciences). Before imaging, the mice were shaved and anesthetized. IVIS measurements (exposure time: 120 seconds, binning factor: 16, aperture: f/1.2) were performed 8 minutes after subcutaneous injection of D-luciferin in the neck (100 mg/kg in PBS; Caliper Life Sciences). The liver load was quantified measuring total flux (p/s) of an ROI covering the liver (same ROI for all mice). Image analysis was performed using the Living Image® 4.4 software (Perkin Elmer Life Sciences). Infected mice were monitored for blood stage infections by Giemsa-stained blood smear until day 9 post infection. The prepatent period (measured in days after SPZ challenge) was defined as the first day at which blood stage infection with a parasitemia of >0.5% was observed.

Quantification of sporozoites by PCR

Directly after SPZ delivery by 32 (IQR: 32-33) mosquito bites of which 18 (IQR: 17-19) contained blood, the skin of 4 exposed mice was cut out, snap-frozen and stored at -20 °C until further use. Parasite burden was measured by quantitative real-time reverse transcription polymerase chain reactions (qRT-PCR). The DNA was extracted from the frozen skin using the QIAamp DNA Micro Kit (Qiagen) following the manufacturer's instruction. Amplification reactions of each DNA sample were performed in PCR plates (hard-shell PCR plate, #HSP9645; Bio-Rad), in a volume of 25 µl containing 12.5 µl PCR buffer (HotstarTaq mastermix; Qiagen), 0.5 µl $MgCl_2$ (25mM), Plasmodium-specific forward and reverse primer (12.5 pmol; Plas-7F 5'-GTTAAGGGAGTGAAGACGATCAGA-3' and Plas-171R 5'-AACCCAAAGACTTTGATTTCTCATAA-3'; Sigma-Aldrich), PhHV-specific forward and reverse primer (15 pmol; PhHV-267S 5'-GGGCGAATCACAGATTGAATC -3' and PhHV-337AS 5'-GCGGTTCCAAACGTACCAA -3'; Biolegio), Plasmodium-specific FAM10 labelled detection probe (2.5 pmol; PP FAM 5'-ACCGTCGTAATCTTAACC-3'; Biolegio), PhHV-specific Cy5 double-labelled detection probe (1.25 pmol; PhHV-305TQ Cy5 5'-TTTTTATGTGTCCGCCACCATCTGGATC-3'-BHQ2; Biolegio) and 5 µl of the DNA sample (dilution factor: 10x). Amplification consisted of 15 min at 95°C followed by 50 cycles of 15 s at 95°C, 30 s at 60°C, and 30 s at 72°C. Amplification, detection, and analysis were performed with the CFX96TM real-time PCR detection system (Bio-Rad). A calibration curve to assess the SPZ numbers in the mosquito inoculation samples was generated by analyzing skin samples injected with a dilution range of SPZ (2-step dilution, start: 20.000 SPZ, 10 samples, n=3 performed *in duplo*, Figure 1C).

***Ex vivo* (fluorescent) imaging of the dermal site**

Immediately after SPZ delivery, the exposed skin of 8 mice (4 ^{msq}SPZ and 4 ^{syr}SPZ samples) was excised, covered with a cover slip and imaged using an Andor Dragonfly 500 spinning disk confocal on a Leica DMi8 microscope (Oxford Instruments) or a Leica True Confocal Scanning SP8 microscope (Leica Microsystems). The mCherry expressed by SPZ was excited with the 561nm laser. A 20x objective (HC PL APO 20x/0.75 IMM CORR CS2) was used, resulting in images of 617 x 617 µm. The experiments were performed within 1.5 h after tissue excision at room temperature.

To create overview images of the dermal site, up to 570 fields of views were stitched using the Andor imaging software Fusion (Oxford Instruments). Z-slices were imaged covering an average total depth of 124 µm (IQR: 103-131). Using the Fiji package for the open source software ImageJ[21], the three-dimensional z-stack was reduced into a two-dimensional image using maximum intensity projection (retrieves the level of maximum intensity along the z axis for each x,y position) and was converted into a binary image only showing the SPZ. This image was further processed in two different ways: 1) The Gaussian blur filter was

applied and a pseudo color image was created by applying the inferno color lookup table in Fiji to visualize the location and density of the SPZ, 2) The coordinates of the individual SPZ in the ^{msq}SPZ and ^{syr}SPZ samples were determined and the nearest neighbor distance (distance between the center points of neighboring SPZ) was calculated using the ImageJ Nnd plugin. The blood vessels visible at the brightfield overview image of the dermal site were segmented using the Image Segmenter app available within MATLAB (MathWorks) and the distance from the SPZ center to the nearest blood vessel was calculated. The number of SPZ residing within or in close proximity to hematomas was determined using circular ROIs with a diameter of 650 µm and around the center of the hematoma. The shape of the cells visible at the zoom-in brightfield images (after mosquito inoculation n=164, after syringe injection n=203) was described by two shape descriptors available within ImageJ, namely roundness: with a value of 1.0 indicating a perfect circle and the Feret's diameter: the longest distance between any two points along the cell membrane.

Sporozoite motility

To analyze SPZ motility, movies were recorded with a frame rate of 35-40 frames per minute, 200 frames per movie. Recording ^{msq}SPZ samples (n=6) yielded a total of 3400 frames. Recording ^{syr}SPZ samples (n=8) yielded a total of 3600 frames. Maximum intensity projections of the recorded microscopy movies were generated using ImageJ. The motility of the SPZ was analyzed using $SMOOT_{mouse\ skin}$, an in-house developed software program, written in the MATLAB programming environment (MathWorks). This tool is an adapted version of the $SMOOT_{human\ skin}$[13, 18] and $SMOOT_{\textit{in vitro}}$[15] tools previously described. Via $SMOOT_{mouse\ skin}$, the SPZ could be segmented per movie frame, based on their fluorescence signal intensity, size and crescent shape. The median pixel locations of the segmented SPZ were connected into full SPZ tracks.

First, the SPZ tracks were characterized as motile or stationary based on their displacement, using a displacement cut-off of 21 pixels which corresponds to the length of a SPZ. Subsequently, the tracks of the motile SPZ were subdivided into defined movement patterns: sharp turn, slight turn and linear segments. Third, for the motile SPZ the mean squared displacement at frame level, the average velocity of their tracks and the nearest neighbor distance per track was calculated and the tortuosity of the tracks was described via the straightness index (the ratio between the total length of the direct path between the start and the end of a track and the total length of the travelled path) and the angular dispersion (the deviation from the mean angle of the track). Finally, the interplay between the angular dispersion, straightness index, velocity and nearest neighbor distance was analyzed, for which the number of ^{msq}SPZ and ^{syr}SPZ tracks within the dataset was equated using random sampling. Twelve subsets of SPZ tracks were defined based on the angular dispersion (<0.5 and >0.5), straightness index (<0.5 and >0.5) and velocity, (<1 µm/s, 1-2 µm/s, >2 µm/s).

Statistical analysis

The average and variability of the data was summarized using the mean and standard deviation (SD) for parametric data or the median and interquartile range (IQR) for nonparametric data. For the comparison of groups, the difference between means or medians was assessed using respectively the independent sample T test and the Mann-Whitney U test. For the comparison of a group with a set value the one sample T test was used. For the comparison of the distribution of categorical data the Chi-squared test was used, including a post hoc analysis based on residuals. A univariate general linear model was used to examine the relationship between a continuous and categorical variable. p-values < 0.05 were considered significant, in case of multiple testing the Bonferroni correction was applied to adjust the p-value. All statistical tests were performed by SPSS Statistics (IBM Nederland BV). To compare the velocity distributions of both groups, the distribution was described performing Expectation-Maximization based fitting. The probability density function that could describe the SPZ velocity distribution consisted of a mixture of 2 normal distributions. The package mixR[22] within the open source R environment[23] was used to define the distribution parameters yielding the best fit.

RESULTS

Infectivity of ^{msq}SPZ and ^{syr}SPZ

At roughly equal numbers of administered ^{msq}SPZ and ^{syr}SPZ, the parasite liver loads of infected mice, assessed by bioluminescence imaging, were 3.5-fold higher in ^{msq}SPZ mice (median: $2.7*10^5$ RLU, IQR: $1.8*10^5$-$3.7*10^5$) as compared to ^{syr}SPZ mice (median: $7.9*10^4$ RLU, IQR: $5.9*10^4$-$8.5*10^4$; p: 0.011; Mann-Whitney U test) (Figure 1). These results were in line with previous reports[8]. The prepatent period of blood stage infection was on average 7 days after infection by mosquito bites. After syringe injection 3/5 mice were still blood slide negative at day 9 after infection, the remaining two mice became positive at day 7 after injection.

Attempts to quantify the number of ^{msq}SPZ by qRT-PCR (Figure 1) showed high variability in estimates (median: 6060, range 2203-13,481), which was at least partly caused by technical variability inherent to DNA extraction from skin lysis samples. The estimated average number of ^{msq}SPZ delivered did not significantly differ from the targeted 3000 (p: 0.205; one-sample t test).

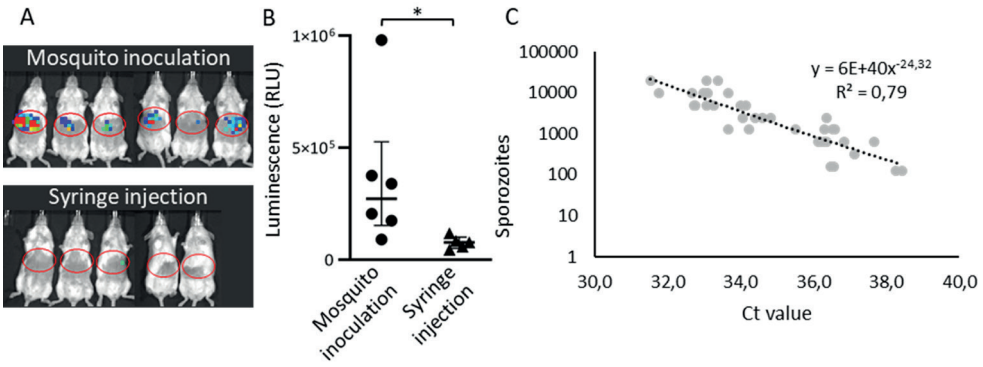

Figure 1 Outcome different administration routes. A) *In vivo* images which show the liver load 44 hr post infection via 33 (IQR: 30-33) mosquito bites or intradermal syringe injection of 3000 SPZ. (B) Average of the luciferase activity in the liver 44 hr after challenge by mosquito inoculation (median: $2.7*10^5$ RLU, IQR: $1.8*10^5$-$3.7*10^5$) or intradermal syringe injection (median: $7.9*10^4$ RLU, IQR: $5.9*10^4$-$8.5*10^4$)(*p=0.011; Mann-Whitney U test). (C) A calibration curve was generated based on a syringe injected concentration range of SPZ in skin (n=3 *in duplo*) to estimate the number of SPZ delivered by 30 mosquito bites (median: 6060 (2203-13,481) SPZ).

Dermal site appearance

The dermal ^{msq}SPZ and ^{syr}SPZ sites were imaged over an average total depth of 124 µm (IQR: 103-131) by confocal microscopy in order to visualize the SPZ distribution. In general, ^{msq}SPZ were distributed both individually and in clusters dispersed throughout the dermal tissue (Figure 2A). We found that ^{msq}SPZ dermal tissue contained multiple hematomas (median number per sample: 6.5). Interestingly we also found hematomas and ^{msq}SPZ in the mouse peritoneum (Sup. Figure S1). Of the ^{msq}SPZ identified, 9% was found within or in close proximity to the hematomas (example is shown in Figure 2Aiv), which represented roughly 23% of the hematomas (6/26). Three quarters of ^{msq}SPZ were found within a 255 µm radius of a blood vessel (Sup. Figure S2).

In contrast, dermal sites containing ^{syr}SPZ showed that the injected medium diffused throughout skin, with a single cluster of ^{syr}SPZ in the centre of this injection site (Figure 2B). Zooming in on the ^{syr}SPZ cluster showed that the ^{syr}SPZ did not agglutinate (Figure 2Bi-iv). We did not find hematomas in the ^{syr}SPZ dermal tissue, nor ^{syr}SPZ in the peritoneum. On average ^{syr}SPZ were located further away from blood vessels, three quarters were found within a 504 µm radius of a blood vessel (Sup. Figure S2; $p<0.001$, Mann Whitney U test). The SPZ distribution was quantified according to their nearest neighbor distance (NND) confirming the dispersed nature of ^{msq}SPZ with a median NND of 55 µm (IQR: 18-132), 5% of the ^{msq}SPZ were further than 376 µm apart (Figure 2C). In contrast, ^{syr}SPZ were clustered at a median NND of 23 µm (IQR: 13-43), 5% of the ^{syr}SPZ were further than 112 µm apart.

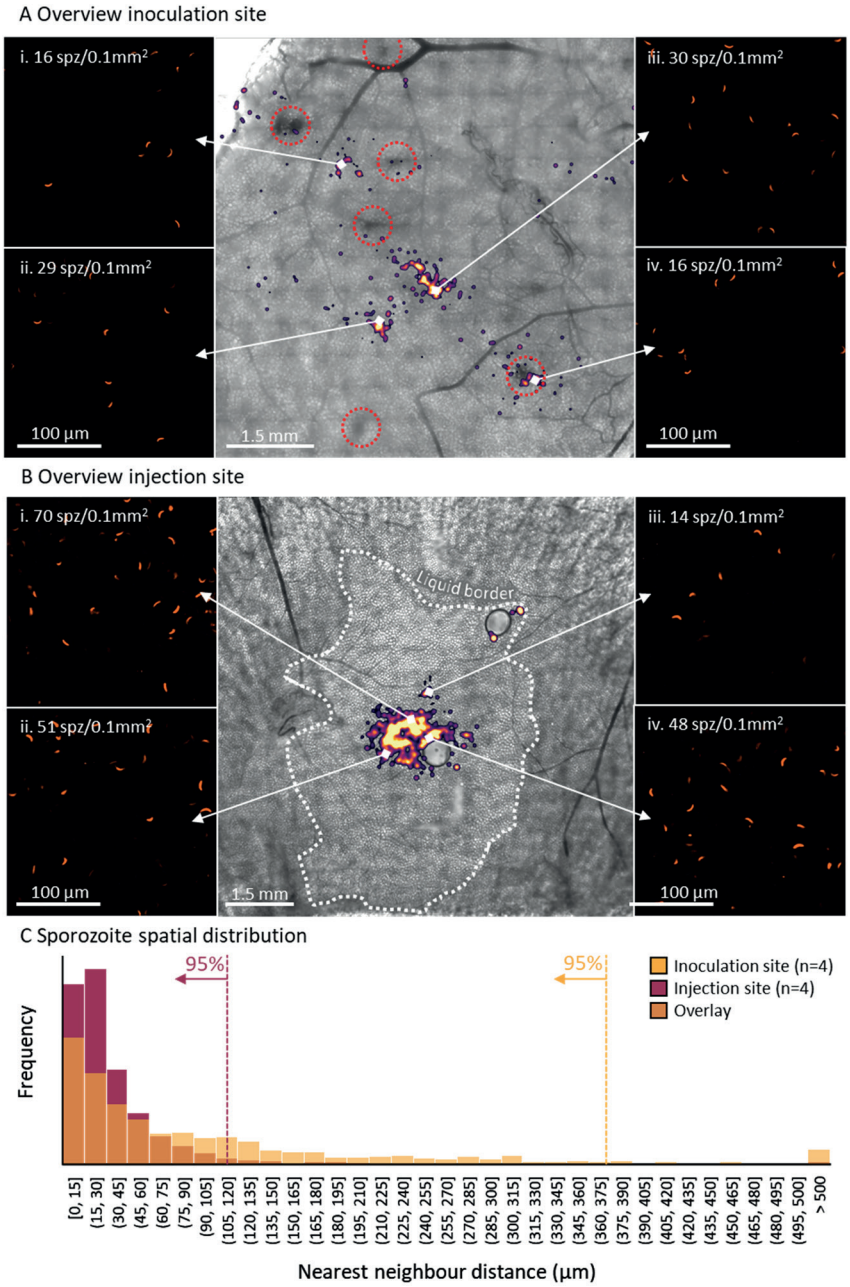

Figure 2 Overview dermal site appearance. A-B) Overview of the inoculation site after SPZ delivery by mosquito (A) and the injection site after SPZ delivery by intradermal syringe injection (B), shown as an overlay of a brightfield image and the SPZ distribution (pseudo-colored, blurred fluorescent image) accompanied by zoom-in images showing the individual SPZ (i-iv). C) Plot of the nearest neighbor distance for ^{msq}SPZ (yellow, median: 55 µm, IQR: 18-132) or ^{syr}SPZ (purple, median: 23 µm, IQR: 13-43), the overlap of both distributions is plotted in orange.

Zooming in on the morphology of the skin tissue, we found that after mosquito inoculation, cells remained densely packed resulting in polygonal shaped cells (mean roundness: 0.75 ± 0.11; Feret's diameter: 82 ± 13 µm) (Figure 3AB). Conversely, after the syringe injection the interstitial space between the cells was enlarged, leading to >15 µm gaps between cells and a change in cell shape towards significantly more rounded cells (mean roundness: 0.87 ± 0.07, p<0.001, independent sample T test; Feret's diameter: 68 ± 10 µm, p<0.001, independent sample T test) (Figure 3AB). The projection of ^{msq}SPZ and ^{syr}SPZ tracks on top of brightfield images showing tissue morphology revealed that the altered tissue morphology was accompanied by altered movement patterns (Figure 3C).

Intradermal sporozoite motility

After delivery, the majority of SPZ displayed tortuous movement through the dermal tissue, representative examples are shown in Figure 4A. In total, the movement of 566 ^{msq}SPZ and 1079 ^{syr}SPZ could be captured and analyzed. Both ^{msq}SPZ and ^{syr}SPZ were equally motile (respectively 89% and 88%). Following both administration routes, the tracks of the SPZ were highly curved. Traditional motility measures such as the mean squared displacement were thus unsuitable to accurately describe the migration behavior of both groups of SPZ (Sup. Figure S3). Therefore, we included other parameters to investigate the tortuous migration behavior. Tracks were color-coded for movement pattern, e.g. straight in red, slight turns in blue, sharp turns in yellow. Both ^{msq}SPZ and ^{syr}SPZ showed equal numbers of turns as compared to straight paths with the percentage turns at frame level at 88% for both samples (Figure 4Bi). The percentage of sharp turns was somewhat decreased in ^{msq}SPZ as compared to ^{syr}SPZ (slight/sharp turns ^{msq}SPZ: 46/42%, ^{syr}SPZ: 34/54%; p<0.001, Chi-square test; Figure 4Bi). Analysis of straightness index (Figure 4Biii), revealed a similarly high level of tortuosity in both conditions (median straightness index ^{msq}SPZ: 0.24, IQR: 0.09-0.53; ^{syr}SPZ: 0.28, IQR: 0.14-0.56; p=0.14, Chi-square test). Turns were made both clockwise (CW) and counter CW (CCW), with a slight preference for CCW in the ^{msq}SPZ group (CW ^{msq}SPZ: 40%, ^{syr}SPZ: 51%; CCW ^{msq}SPZ: 60%, ^{syr}SPZ: 49%; p<0.001, Chi-square test) (Figure 4Bii). Interestingly, the turn angle of ^{msq}SPZ was much more consistent, described by angular dispersion (Figure 4Biv), as compared to ^{syr}SPZ (median angular dispersion ^{msq}SPZ: 0.74, IQR: 0.54-0.87; ^{syr}SPZ: 0.58, IQR: 0.32-0.77; p<0.001, Chi-square test). In conclusion, both ^{msq}SPZ and ^{syr}SPZ travelled highly tortuous paths, whereby ^{msq}SPZ showed less sharp turns, a more consistent turn angle and a predominance for the well-described preferred CCW turn angle.

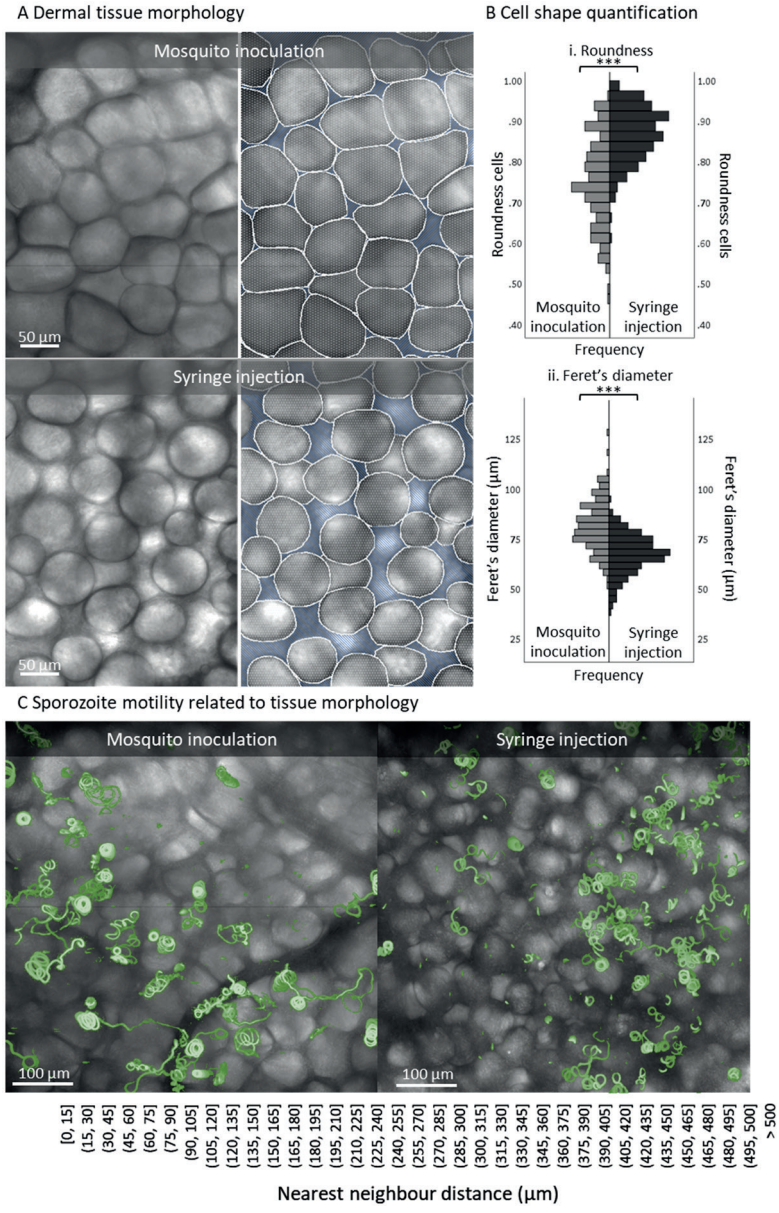

Figure 3 Zoom-in on dermal tissue morphology after sporozoite delivery. A) Zoom-in on the tissue morphology of the inoculation site after SPZ delivery by mosquito and the injection site after SPZ delivery by intradermal syringe injection. Based on the brightfield images, the cells (depicted in white) and the interstitial space (depicted in blue) were segmented. B) Quantification of the cell shapes found after mosquito inoculation (n=164) and syringe injection (n=203) using roundness (i) and the Feret's diameter (the longest distance between any two points along the cell membrane) (ii) as measures. ***p<0.001; independent sample T test. C) Overview of the dermal site shown as an overlay of a brightfield image and a map of mosquito-inoculated and syringe-injected SPZ tracks (depicted in green).

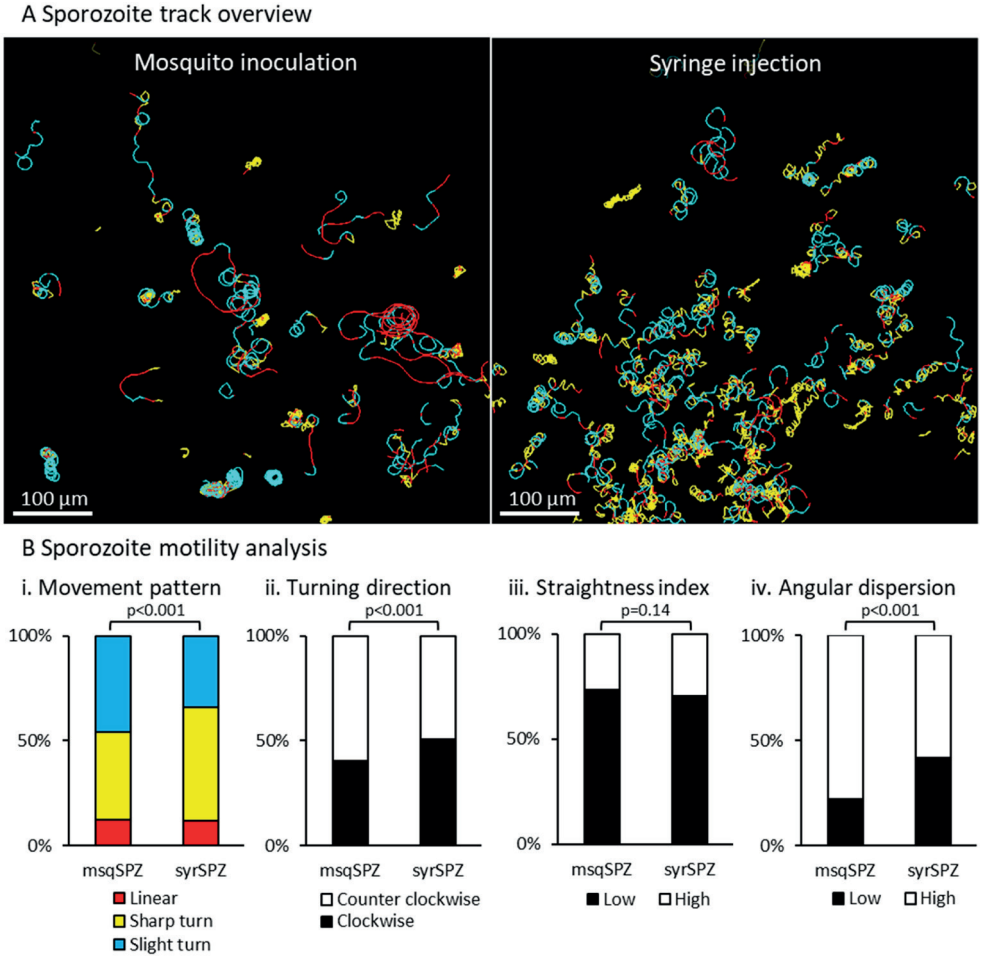

Figure 4 Movement pattern of sporozoites. A) Overview of the inoculation site after SPZ delivery by mosquito and the injection site after SPZ delivery by intradermal syringe injection, shown as a map of SPZ tracks, color-coded for movement pattern (sharp turns in yellow, slight turns in blue, linear movement in red). B) Quantification of the different aspects of SPZ motility after administration by mosquito or syringe: (i) The movement pattern distribution based at frames, (ii) the percentage of clockwise and counter clockwise segments (iii) the straightness index of the tracks (low: <0.5, high: >0.5) and (iv) the angular dispersion of the tracks (low: <0.5, high: >0.5). p-values obtained by Chi-square test.

SPZ velocity fluctuated along tracks (visualized by color-coding in Figure 5A), which was in line with earlier findings[15, 18, 24, 25]. Plotting the average track-velocities revealed a distribution that could be described with a mixture of two normal distributions (Figure 5B). The first peak was comparable for both administration routes and contained the slow moving ^{msq}SPZ and ^{syr}SPZ with a mean velocity of respectively 1.0 ± 0.4 and 0.9 ± 0.2 µm/s. The second peak, containing the highly viable and rapid ^{msq}SPZ and ^{syr}SPZ, differed between the administration routes at a mean of 2.4 ± 0.7 µm/s for ^{msq}SPZ and 1.7 ± 0.6 µm/s for ^{syr}SPZ. Thus, the rapid ^{msq}SPZ moved on average 1.4-fold faster than the ^{syr}SPZ.

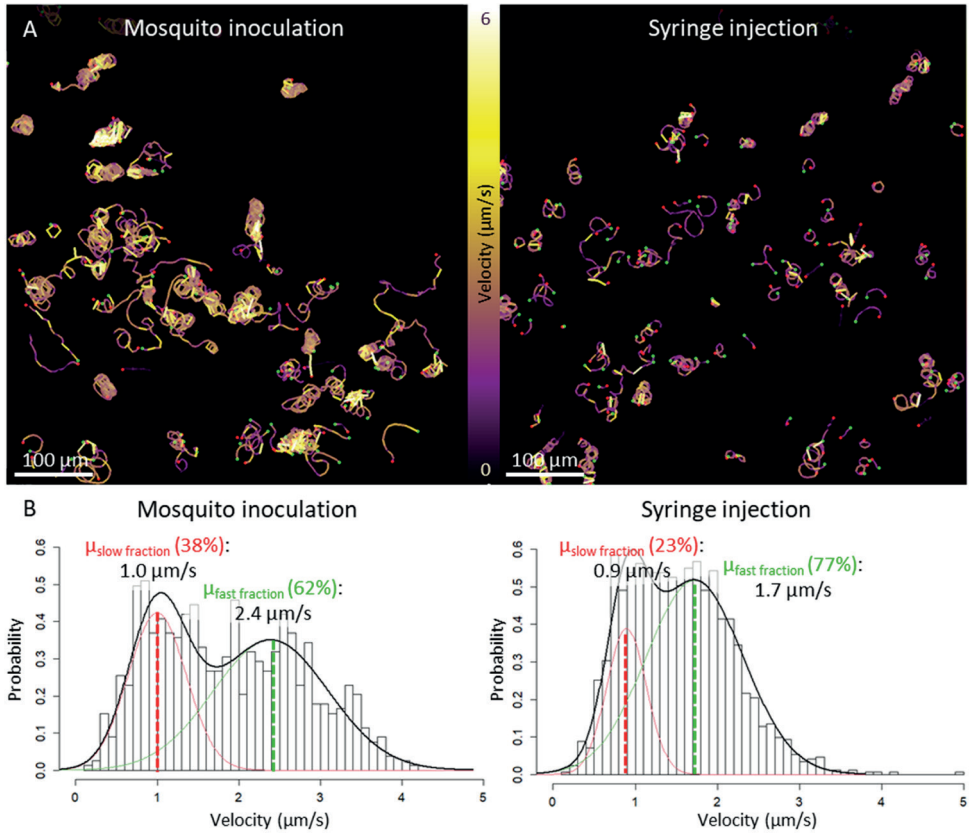

Figure 5 Velocity of sporozoites. A) Overview of the inoculation site after SPZ delivery by mosquito inoculation and the injection site after SPZ delivery by intradermal syringe injection, shown as a map of SPZ tracks, color-coded for velocity (yellow sections corresponded to a high velocity, purple sections, corresponded to a lower velocity) (B) The distribution of the average track velocity including a probability density function with its mean determined using expectation-maximization based fitting of a mixture of 2 normal distributions; one describing the slow moving SPZ fraction (depicted in red, accounting for 38% of the ^{msq}SPZ and 23% of the ^{syr}SPZ) and one describing the fast moving SPZ fraction (depicted in green, accounting for 62% of the ^{msq}SPZ and 77% of the ^{syr}SPZ).

Interplay between motility parameters

To obtain a multidimensional view of SPZ migration, we explored the relationship between tortuosity parameters. Based on high and low straightness index (SI) and angular dispersion (AD), the SPZ tracks could be divided into four typical movement patterns: short erratic tracks (low AD, high SI), short straight tracks (high AD, high SI), consistently turning tracks (high AD, low SI) and erratically turning tracks (low AD, low SI) (Figure 6A). Representative examples of tracks from these groups are shown in Figure 6B. The majority of the tracks (49%) were classified as consistently turning (49%), which typically is the 'default' movement pattern which SPZ display *in vitro* (Figure 6A).

We subsequently investigated the relationship between the four movement patterns and velocity. We found that consistently turning tracks were generally rapid SPZ (median 2.0 µm/s, IQR 1.5-2.6), whereas erratically turning SPZ were considerably slower (median: 1.2 µm/s, IQR 0.9-1.7; $p<0.001$, Mann-Whitney U test). Interestingly, these consistently turning rapid SPZ were overrepresented within the ^{msq}SPZ group as compared to the ^{syr}SPZ group (2.4-fold difference), which was offset by a reciprocal increase in slower erratically turning SPZ within the ^{syr}SPZ group (2.5-fold difference) ($p<0.001$, Chi-square test) (Figure 6D).

Lastly, we determined if the distribution of the SPZ as reflected by the nearest neighbor distance (NND) influenced the tortuosity and velocity of their tracks. In general, the average NND of ^{msq}SPZ was larger compared to ^{syr}SPZ as was observed by the analysis of the individual parameters (Figure 2, Sup. Figure S4). However, this difference was consistent among all different movement patterns ($p=0.52$; interaction term $^{msq/syr}$SPZ * subsets, univariate general linear model), which suggested that the movement pattern or velocity of SPZ was not dependent on their interindividual distance. Taken together, the ^{syr}SPZ group contained more SPZ that exhibited erratic movement at a slower speed, whereas the ^{msq}SPZ group contained more SPZ that circled consistently at high speed.

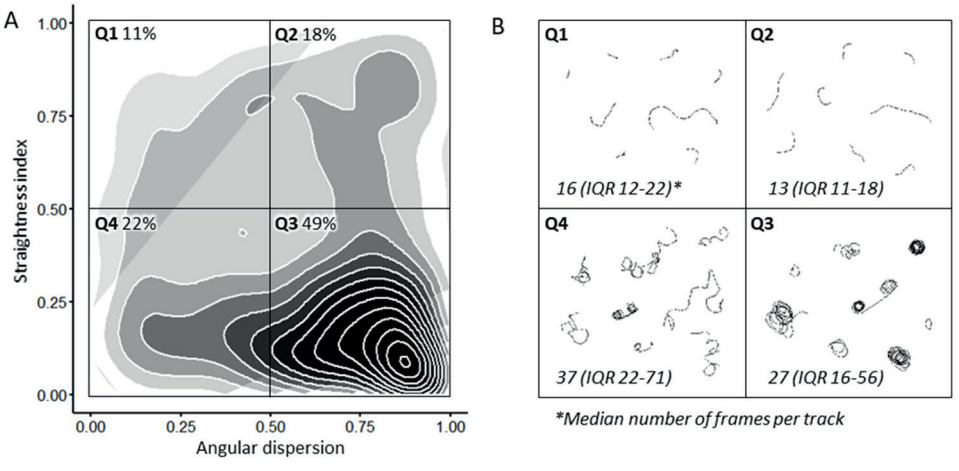

D

(%)	S1	S2	S3	S4	S5	S6	S7	S8	S9	S10	S11	S12
msqSPZ	4.9	6.4	x	5.8	x	8.5	19.5	6.0	x	x	35.5	x
syrSPZ	8.2	3.7	x	9.9	x	11.6	22.9	15.3	x	x	14.7	x

Figure 6 Interplay between motility parameters. A) Density plot of all SPZ tracks (including both ^{msq}SPZ (n=778) and ^{syr}SPZ (n=778) in a matrix of angular dispersion and the straightness index. B) Representative example movement patterns associated with every quarter of the density plot. Group Q1: low angular dispersion, high straightness index (short, erratic tracks); Q2: high angular dispersion, high straightness index (short, straight tracks); Q3: high angular dispersion, low straightness index (consistently turning tracks); Q4: low angular dispersion, low straightness index (erratically turning tracks). C) Density plot of all low (i), intermediate (ii) and high (iii) velocity tracks on the same matrix of angular dispersion and straightness index, resulting in twelve subsets (S1-12). Velocity categories are defined as: slow <1 µm/s (depicted in purple), intermediate 1-2 µm/s (depicted in orange) and fast >2 µm/s (depicted in yellow). Percentage of the overall number of SPZ tracks in every quarter of the density plots are given. D) Comparison of the distribution (as a percentage of total tracks) for ^{msq}SPZ and ^{syr}SPZ tracks across subsets S1-12, with significant differences between S8 and S11 ($p<0.001$, Chi-square test).

DISCUSSION

Using confocal microscopy and dedicated SPZ imaging software, we visualized SPZ deposited by mosquito inoculation or syringe injection and assessed quantitative differences. We found that delivery via syringe injection decreases infectivity of SPZ by roughly three-fold as compared to mosquito inoculation, which is related to 1) a clustered distribution of ^{syr}SPZ through the skin with larger distance to blood vessels, 2) a lack of hematomas, which are typically induced by mosquito bites, 3) enlarged interstitial space due to the syringe injection of fluid, 4) slower and more erratic migration patterns of ^{syr}SPZ as compared to ^{msq}SPZ. Each of these parameters could impact the efficiency of SPZ migration, blood vessel invasion and ultimate liver infectivity and thus provide important insights on how to critically improve delivery of SPZ-based vaccines.

The dispersed distribution of ^{msq}SPZ and the fact that a substantial proportion of ^{msq}SPZ is deposited close to hematomas created by mosquito probing[26, 27] provide them with better odds of finding blood stream access as compared to ^{syr}SPZ. This is in line with the consistent circular motility of ^{msq}SPZ, which has previously been associated with increased blood vessel engagement[14, 17]. However, in previous publications, this engagement was generally related to deceleration, while in our study consistent circular motility was related to high velocities[14, 17]. Conversely, the slower erratic movement of ^{syr}SPZ is most likely caused by the alteration of physical space as a consequence of fluid injection. SPZ movement is strongly guided by their three-dimensional environment; without any confinement, SPZ *in vitro* display a continuous, preferential counter-clockwise movement pattern[15, 24], while *in vivo*, skin structure redirects SPZ to display much more complex patterns[16, 18]. The role of physical confinement has been further supported by experiments whereby micropatterned *in vitro* environments were created that could induce specific movement patterns of SPZ[28]. We clearly found that the liquid co-injected with the ^{syr}SPZ widened the interstitial space, which allows ^{syr}SPZ to display erratic movement patterns.

Despite the fact that mouse skin does not fully replicate human skin regarding skin thickness (mouse skin <1 mm vs human skin >2 mm[29]), as underlined by ^{msq}SPZ deposition in the mouse peritoneum (length of mosquito proboscis: 1.5-2.0 mm[30]), the remarkable differences between the ^{msq}SPZ and ^{syr}SPZ dermal sites provide important clues on how to critically improve intradermal syringe injections of attenuated SPZ vaccines. Particularly, a microneedle (patch), tattoo device or Nanoliter Injector may be useful to not only create the relevant SPZ dispersion, but also to decrease injection volume to the nanoliter range[31-35]. In addition, laser-induced vascular damage can potentially mirror the hematomas induced by mosquito probing and enhance the blood vessel entrance of ^{syr}SPZ[36]. Recently, this concept was successfully applied to increase parasite loads in the liver after intradermal syringe injection[37].

Importantly, our study demonstrates that state-of-the-art imaging (analysis) techniques can provide valuable quantitative assessments of parameters affecting SPZ migration. Our *ex vivo* set-up combined with spinning-disk confocal microscopy and SPZ tracking software enabled 1) the visualization of (the SPZ distribution throughout) the whole inoculation and injection site (up to 100 mm^2), whereas up to now only one field of view (<0.5 mm^2) was visualized during *in vivo* live imaging[14, 17, 38], 2) the visualization of morphological tissue deformation as a result of the fluid injection, previously acknowledged as an important parameter regarding transdermal drug delivery[39-41], but not yet visualized at a micron level resolution and 3) a multidimensional analysis of SPZ motility unveiling an remarkable interplay between motility parameters which were up to now only studied independently[16-18]. Further research is needed to study the role of other potential contributors not accounted for in this imaging study, such as their pre-processing of ^{syr}SPZ (manual extraction from salivary glands in culture medium) and the effect of saliva inoculated by mosquitoes[15, 42, 43]. Our quantitative assessment of parameters affecting SPZ migration 1) indicates that engineering solutions should be explored that can better mimic mosquito inoculation as well as 2) provides a readout needed to assess the potential of the suggested engineering solutions. In conclusion, detailed microscopic imaging of the dermal site appearance and migration patterns of SPZ revealed important quantitative differences between SPZ administration via mosquito inoculation vs intradermal syringe injection. These findings open new avenues for intradermal delivery of attenuated SPZ vaccines with enhanced efficacy.

Acknowledgments: We would like to thank ing. J. Ramesar and dr. C.J. Janse for support with the mosquito infection. We also thank the light microscopy facility team of the LUMC for their support during image acquisition and analysis.

REFERENCES

1. Organization, W.H., World Malaria Report 2019. 2019.
2. Richie, T.L., et al., Progress with Plasmodium falciparum sporozoite (PfSPZ)-based malaria vaccines. Vaccine, 2015. 33(52): p. 7452-61.
3. Clyde, D.F., Immunity to Falciparum and Vivax Malaria Induced by Irradiated Sporozoites - a Review of the University-of-Maryland Studies, 1971-75. Bulletin of the World Health Organization, 1990. 68: p. 9-12.
4. Hoffman, S.L., et al., Protection of humans against malaria by immunization with radiation-attenuated Plasmodium falciparum sporozoites. J Infect Dis, 2002. 185(8): p. 1155-64.
5. Epstein, J.E., et al., Live attenuated malaria vaccine designed to protect through hepatic CD8(+) T cell immunity. Science, 2011. 334(6055): p. 475-80.
6. Seder, R.A., et al., Protection against malaria by intravenous immunization with a nonreplicating sporozoite vaccine. Science, 2013. 341(6152): p. 1359-65.
7. Ploemen, I.H.J., et al., Visualisation and Quantitative Analysis of the Rodent Malaria Liver Stage by Real Time Imaging. Plos One, 2009. 4(11).
8. Haeberlein, S., et al., Protective immunity differs between routes of administration of attenuated malaria parasites independent of parasite liver load. Sci Rep, 2017. 7(1): p. 10372.
9. Nganou-Makamdop, K., et al., Reduced Plasmodium berghei sporozoite liver load associates with low protective efficacy after intradermal immunization. Parasite Immunology, 2012. 34(12): p. 562-569.
10. Nussenzweig, R.S., et al., Protective Immunity Produced by Injection of X-Irradiated Sporozoites of Plasmodium Berghei. Nature, 1967. 216(5111): p. 160-+.
11. Ploemen, I.H., et al., Plasmodium liver load following parenteral sporozoite administration in rodents. Vaccine, 2013. 31(34): p. 3410-3416.
12. Natarajan, R., et al., Fluorescent Plasmodium berghei sporozoites and pre-erythrocytic stages: a new tool to study mosquito and mammalian host interactions with malaria parasites. Cellular microbiology, 2001. 3(6): p. 371-379.
13. Winkel, B.M.F., et al., A tracer-based method enables tracking of Plasmodium falciparum malaria parasites during human skin infection Theranostics, 2019. 9(10): p. 2768-2778.
14. Amino, R., et al., Quantitative imaging of Plasmodium transmission from mosquito to mammal. Nat Med, 2006. 12(2): p. 220-4.
15. de Korne, C.M., et al., Regulation of Plasmodium sporozoite motility by formulation components. Malaria Journal, 2019. 18.
16. Hellmann, J.K., et al., Environmental constraints guide migration of malaria parasites during transmission. PLoS Pathog, 2011. 7(6): p. e1002080.
17. Hopp, C.S., et al., Longitudinal analysis of Plasmodium sporozoite motility in the dermis reveals component of blood vessel recognition. Elife, 2015. 4.
18. Winkel, B.M.F., et al., Quantification of wild-type and radiation attenuated Plasmodium falciparum sporozoite motility in human skin. Scientific Reports, 2019. 9.
19. Sinden, R., Infection of mosquitoes with rodent malaria, in The Molecular Biology of Insect Disease Vectors, C.B.B.a.C.L. J. M. Crampton, Editor. 1997, Springer, Dordrecht. p. 67-91.
20. Kebaier, C., Y. Jin, and J. Vanderberg, Direct microscopic quantification of transmission dynamics of Plasmodium sporozoites from mosquitoes to mice. American Journal of Tropical Medicine and Hygiene, 2007. 77(5): p. 11-12.
21. Schindelin, J., et al., Fiji: an open-source platform for biological-image analysis. Nature Methods, 2012. 9(7): p. 676-682.
22. Yu, Y., mixR: Finite Mixture Modeling for Raw and Binned Data. 2018.
23. R Core Development Team, R: A language and environment for statistical computing. 2020, R Foundation for Statistical Computing: Vienna, Austria.
24. Hegge, S., et al., Automated classification of Plasmodium sporozoite movement patterns reveals a shift towards productive motility during salivary gland infection. Biotechnol J, 2009. 4(6): p. 903-13.
25. Munter, S., et al., Plasmodium sporozoite motility is modulated by the turnover of discrete adhesion sites. Cell Host Microbe, 2009. 6(6): p. 551-62.
26. Choumet, V., et al., Visualizing Non Infectious and Infectious Anopheles gambiae Blood Feedings

in Naive and Saliva-Immunized Mice. Plos One, 2012. 7(12).
27. Vanderberg, J.P., Imaging mosquito transmission of Plasmodium sporozoites into the mammalian host: Immunological implications. Parasitology International, 2014. 63(1): p. 150-164.
28. Muthinja, M.J., et al., Microstructured Blood Vessel Surrogates Reveal Structural Tropism of Motile Malaria Parasites. Adv Healthc Mater, 2017. 6(6).
29. Wei, J.C.J., et al., Allometric scaling of skin thickness, elasticity, viscoelasticity to mass for micro-medical device translation: from mice, rats, rabbits, pigs to humans. Scientific Reports, 2017. 7.
30. Ramasubramanian, M.K., O.M. Barham, and V. Swaminathan, Mechanics of a mosquito bite with applications to microneedle design. Bioinspiration & Biomimetics, 2008. 3(4).
31. Crichton, M.L., et al., The changing shape of vaccination: improving immune responses through geometrical variations of a microdevice for immunization (vol 6, 27217, 2016). Scientific Reports, 2016. 6.
32. Esser, E.S., et al., Microneedle patch delivery of influenza vaccine during pregnancy enhances maternal immune responses promoting survival and long-lasting passive immunity to offspring. Scientific Reports, 2017. 7.
33. Quinn, H.L., et al., The role of microneedles for drug and vaccine delivery. Expert Opinion on Drug Delivery, 2014. 11(11): p. 1769-1780.
34. Shio, M.T., et al., Drug Delivery by Tattooing to Treat Cutaneous Leishmaniasis. Scientific Reports, 2014. 4.
35. Atif, M., J.W. Lynch, and A. Keramidas, The effects of insecticides on two splice variants of the glutamate-gated chloride channel receptor of the major malaria vector, Anopheles gambiae. British Journal of Pharmacology, 2020. 177(1): p. 175-187.
36. Sklar, L.R., et al., Laser Assisted Drug Delivery: A Review of An Evolving Technology. Lasers in Surgery and Medicine, 2014. 46(4): p. 249-262.
37. Zhou, C., et al., Laser mimicking mosquito bites for skin delivery of malaria sporozoite vaccines. Journal of Controlled Release, 2015. 204: p. 30-37.
38. Vanderberg, J.P. and U. Frevert, Intravital microscopy demonstrating antibody-mediated immobilisation of Plasmodium berghei sporozoites injected into skin by mosquitoes. Int J Parasitol, 2004. 34(9): p. 991-6.
39. Gupta, J., et al., Infusion pressure and pain during microneedle injection into skin of human subjects. Biomaterials, 2011. 32(28): p. 6823-6831.
40. Mansoor, I., et al., A microneedle-based method for the characterization of diffusion in skin tissue using doxorubicin as a model drug. Biomedical Microdevices, 2015. 17(3).
41. Shrestha, P. and B. Stoeber, Fluid absorption by skin tissue during intradermal injections through hollow microneedles. Scientific Reports, 2018. 8.
42. Doolan, D.L., Malaria Methods and Protocols. 2002: Humana Press Inc.
43. Schleicher, T.R., et al., A mosquito salivary gland protein partially inhibits Plasmodium sporozoite cell traversal and transmission. Nature Communications, 2018. 9.

SUPPLEMENTARY INFORMATION

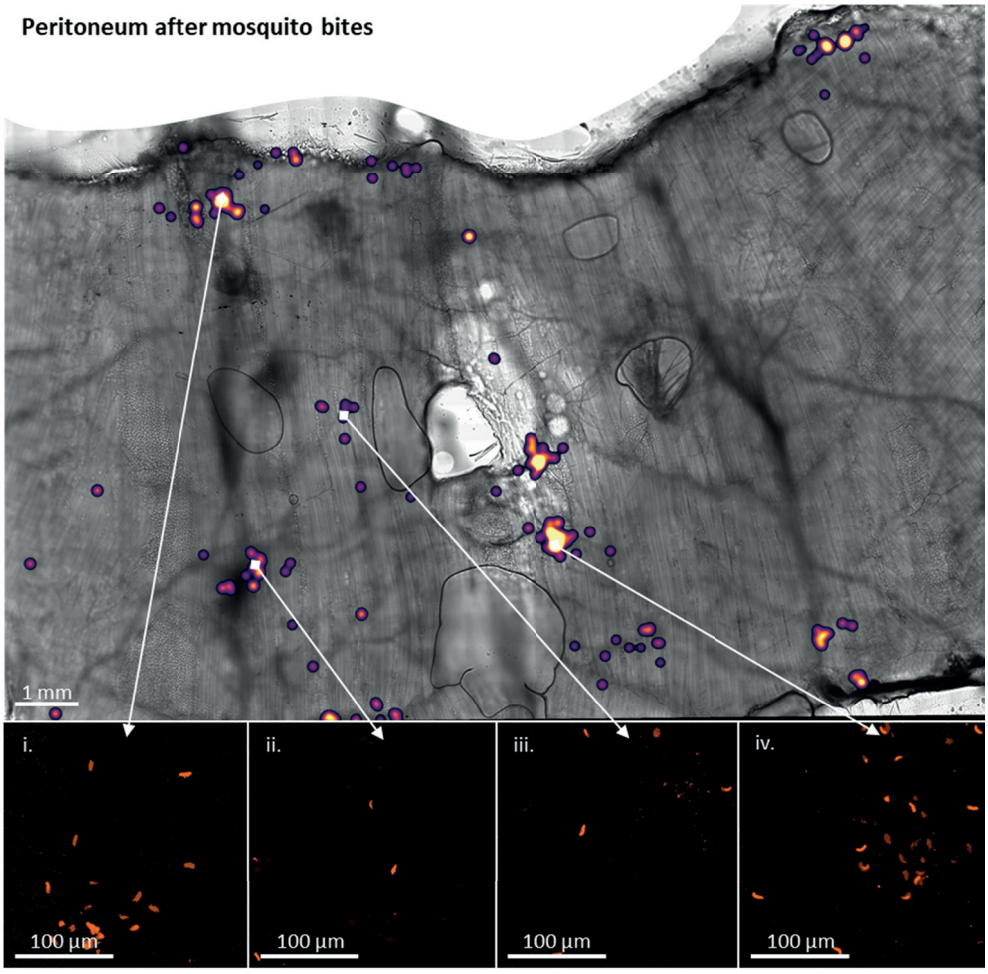

Sup. Figure S1 Peritoneum after mosquito bites. Overview of peritoneum after SPZ delivery by mosquito inoculation shown as an overlay of a brightfield image and the SPZ distribution accompanied by zoom-in images showing the individual SPZ (i-iv).

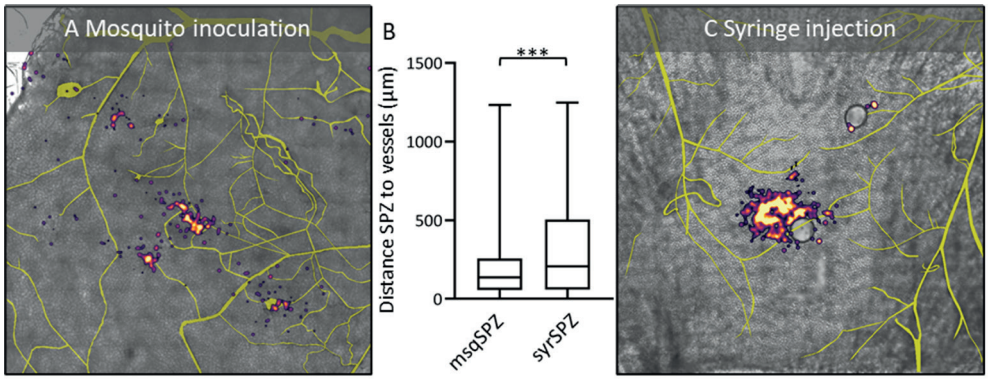

Sup. Figure S2 Sporozoite to blood vessel distance. A & C) Overview of the inoculation site after SPZ delivery by mosquito (A) and the injection site after SPZ delivery by intradermal syringe injection (C) shown as an overlay of a brightfield image, the SPZ distribution (pseudo-colored, blurred fluorescent image) and the segmented blood vessels (depicted in yellow). B) Quantification of the SPZ-to-blood vessel distance (n=2 per condition). ***p<0.001; Mann Whitney U test.

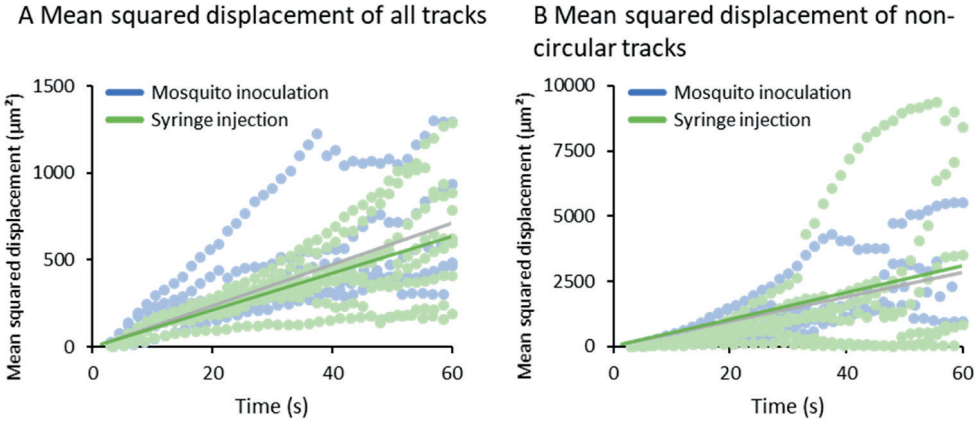

Sup. Figure S3 Mean squared displacement. A-B) The mean squared displacement of the SPZ after administration by mosquito inoculation or syringe injection is plotted. In A) all tracks are included, in B) the circular tracks are excluded (90% of mosquito inoculation frames, 95% of syringe injection frames). The mean squared displacement of the individual samples is plotted as a dotted line, a linear trendline is plotted as a solid line.

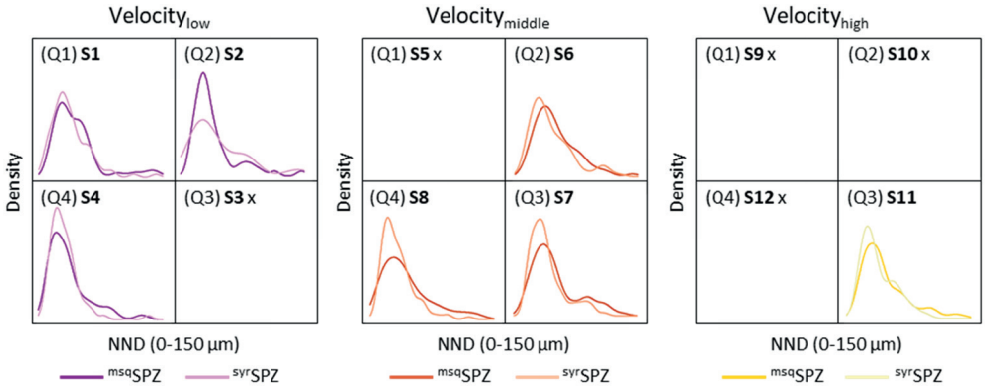

Sup. Figure S4 Relation between motility parameters and nearest neighbor distance. The nearest neighbor distance (NND) is plotted for the tracks split into 12 subsets (S1-12) based on four specific movement patterns (Q1-4, see Figure 6) and three velocity categories (1: <0.1 µm/s, depicted in purple; 2: 1-2 µm/s, depicted in orange; 3: >2 µm/s, depicted in yellow). The NND of the ^{msq}SPZ is depicted in the darker color and the NND of the ^{syr}SPZ in depicted in the lighter color.